Neutron-scattering evidence for the coupling of shear and reorientational motions in the viscoelastic liquid quinoline

F. J. Bermejo and M. García-Hernández
Instituto de Estructura de la Materia, Consejo Superior de Investigaciones Científicas, Serrano 123, E-28006 Madrid, Spain

W. S. Howells
ISIS Pulsed Neutron Facility, Rutherford Appleton Laboratory, Chilton, Didcot, Oxon OX11 0QX, United Kingdom

R. Burriel
Instituto de Ciencia de Materiales de Aragón, Consejo Superior de Investigaciones Científicas, Facultad de Ciencias, Ciudad Universitaria, E-50009 Zaragoza, Spain

F. J. Mompeán
Instituto de Estructura de la Materia, Consejo Superior de Investigaciones Científicas, Serrano 123, E-28006 Madrid, Spain

D. Martin
ISIS Pulsed Neutron Facility, Rutherford Appleton Laboratory, Chilton, Didcot, Oxon OX11 0QX, United Kingdom
(Received 4 June 1993)

The anomalous behavior of several thermal and dynamical properties of liquid quinoline within the temperature range of $260 \leq T \leq 310$ K is investigated. The neutron quasielastic scattering spectra are analyzed using, for the purpose, previous dynamical information available from NMR relaxation and depolarized light scattering. The temperature dependence of the mass-diffusion and reorientational coefficients is derived from the experimental data, evidencing that only the rotational motion shows a clear deviation from Arrhenius behavior. The presence of shear wave excitations which couple to reorientational motions is manifested as a strong inelastic background which shows a marked wave-vector dependence.

PACS number(s): 61.20.Lc

I. INTRODUCTION

The existence of thermal anomalies at temperatures within the normal liquid phase of a large number of (mostly) organic glass formers as revealed by calorimetric and susceptibility measurements within the hydrodynamic range (light-scattering, NMR, etc.) seems to be nowadays a well-established fact [1–3]. In this respect, liquid salol and quinoline have constituted, for more than two decades, an interesting benchmark where phenomenological approximations cast in terms of macroscopic transport coefficients seemed to be at odds with the experimental measurements. As a matter of fact, both liquids show the presence of noticeable (quinoline) or strong (salol) shear wave excitations at low temperatures [4–6] with a frequency dispersion which also shows a considerable dependence with temperature [4]. Such facts, which could not be accounted for by simplified generalized hydrodynamics developments, generated a substantial theoretical effort [1] which, cast in form of the Mori-Zwanzig projection operator technique [7] or linear irreversible thermodynamics [8], can account for the strong temperature dependence of the depolarized (I_V^H or I_H^V) Rayleigh-Brillouin spectra in terms of the oscillation and relaxation of the shear modes which couple to collective reorientational motions in order to relieve the microscopic stresses generated within the liquid.

The case of liquid quinoline is paramount since, apart from evidencing the presence of shear excitations [4,5] at high temperatures (253–320 K) with a well-defined transition between propagative and diffusive regimes [5], a well-defined anomaly was found by several macroscopic properties such as the heat capacity, NMR relaxation times, or even magnetic susceptibility measurements [3]. What is even more remarkable is the fact that such an anomaly could not be found in a closely related chemical analog (isoquinoline), thus indicating a clear microscopic origin of the measured behavior.

The purpose of the present work is therefore to assess whether such an anomaly can be traced down to microscopic scales, using for the purpose high-resolution quasielastic neutron scattering, as well as the previous data from other sources.

A brief description of the experimental and data analysis procedures is given in Sec. II, and the main results are described in Sec. III. The relevance of the present findings are discussed in Sec. IV and the main conclusions are finally given in Sec. V.

II. EXPERIMENTAL AND COMPUTATIONAL DETAILS

A. Experiments

The experimental neutron quasielastic measurements were carried out using the IRIS high-resolution spec-

trometer located at one of the neutron guides of the ISIS spallation neutron source of the Rutherford Appleton Laboratory. The sample was obtained from a commercial purveyor (Merck purity 99) and was used without further purification. For the neutron measurements, the sample cell was formed by two aluminum foils of 0.05 mm separated by a spacer of 0.5 mm (sample thickness) which was mounted on a standard (orange) cryostat. The spectra were measured for several temperatures covering the liquid range (250–310 K) as well in the frozen state, which served as a standard reference. Both pyrolitic graphite (002) (PG002) and mica (006) (MI006) reflections were used in order to cover a momentum-transfer range of $0.4 \leq Q \leq 1.7$ Å^{-1}. The resolution in energy transfer estimated from vanadium runs as well as from the deeply frozen sample was about 5.5 μeV (half width at half maximum) for PG(002) and about 5.1 μeV for MI(006).

The experimental data processing was carried out using the IDA set of computer programs [9]. The absorption corrections were applied using the SLABS code [10], and the multiple-scattering contributions were evaluated from Monte Carlo calculations performed with the DISCUS code [11], employing for the purpose scattering kernels based upon rotational diffusion models for which the relevant parameters were estimated following procedures delineated in Sec. II B. The maximum percentage of multiply scattered neutrons never exceeded 10%. The corrected spectra were than converted into constant Q by means of a modification of the INGRID code [12] performed in order to adapt this code for inverted geometry spectrometers. A sample of corrected spectra corresponding to temperatures at both sides of the reported anomaly is shown in Fig. 1 for three representative values of the momentum-transfer.

In order to ascertain whether any structural change in the microscopic short-range order within the liquid phase takes place within this temperature interval, the x-ray-diffraction spectra for a set of representative temperatures at both sides of the anomaly were measured using a Guinier diffractometer (Huber 644) operating with a Cu $K\alpha_1$ beam issued from a germanium monochromator. The sample was held in a rotating Lindemann glass capillary (inside diameter $dd = 1$ mm) and the temperature was maintained constant along the capillary to within ± 1 K with a Cryostream cooler. The diffraction patterns were registered with a scintillation counter.

B. Data analysis

For a mostly incoherent scatterer such as the one we are dealing with ($\sigma_{\text{incoh}}/\sigma_{\text{coh}} = 7.64$), for which the dominant intermolecular interactions can be assumed to be of Lennard-Jones form (supplemented by small electrostatic interactions), the usual approximation of decoupling between orientational motions of different particles can be safely used [13]. After the partial wave expansion of the scattering law, the usual rotational diffusion approach can be followed to write down a model for the temperature-dependent center-of-mass motions and molecular rotations as

$$I_{\text{mod}}^{\text{diff}}(Q,E,T) = \left[f_{\text{incoh}}^2(Q) \frac{\Gamma_t(Q,T)}{E^2 + 2[\Gamma_t(Q,T)]^2} + \sum_l \chi_l(Q)(2l+1) \frac{\Gamma_r(Q,T)}{E^2 + 2[\Gamma_r(Q,T)]^2} \right], \quad (1)$$

where $f_{\text{incoh}}^2(Q)$ and $\chi_l(Q)$ are molecular form factors given in terms of the distances of the nuclei to the molecular center of mass easily calculable from the known molecular geometry [14], and the model is then specified by the translational and rotational widths

$$\Gamma_t(Q,T) = D_t(T) g(Q) , \quad (2)$$

$$\Gamma_r(Q,T) = \Gamma_t(Q,T) + l(l+1) D_r(T) , \quad (3)$$

in terms of the temperature-dependent translational diffusion $D_t(T)$ and rotational diffusion $D_r(T)$ coefficients, and a function $g(Q)$ which characterizes the wave-vector dependence of the linewidths associated with the long-range diffusion process.

Since there are data from independent experimental means, as illustrated below, enabling the establishment of the temperature dependence of the $D_r(T)$ rotational constants, only the $\Gamma_t(Q,T)$ translational linewidths need to be determined from fits of the observed intensities with a model function such as the one specified above. However, as can be easily gauged from spectra displayed in Fig. 1, the presence of a noticeable temperature- and wave-vector-dependent inelastic background, which at the largest wave vector and high temperatures ($Q = 1.7$ Å^{-1}) becomes the dominant contribution, requires us to supplement the simple diffusional model with a spectral component accounting for this extra intensity. In the absence of any model to represent this intensity, and taking into account that, at these relatively high temperatures, such spectral contributions should arise from heavily damped low-lying excitations (as well as multiexcitations), such a background was modeled as an additional Lorentzian function (an overdamped harmonic oscillator function will show the same shape), so that the total model function to be compared with the experimental intensities becomes

$$I_{\text{mod}}(Q,E,T) = \left[a_{\text{diff}}(T) I_{\text{mod}}^{\text{diff}}(Q,E,T) + a_{\text{inel}}(Q,T) \frac{\Gamma_{\text{inel}}(Q,T)}{E^2 + 2[\Gamma_{\text{inel}}(Q,T)]^2} \right] \otimes R(E) , \quad (4)$$

where $a_{\text{diff}}(T)$ and $a_{\text{inel}}(Q,T)$ are two scaling constants and the model is then convolved with the experimental resolution function $R(E)$. Note that, since the wave-

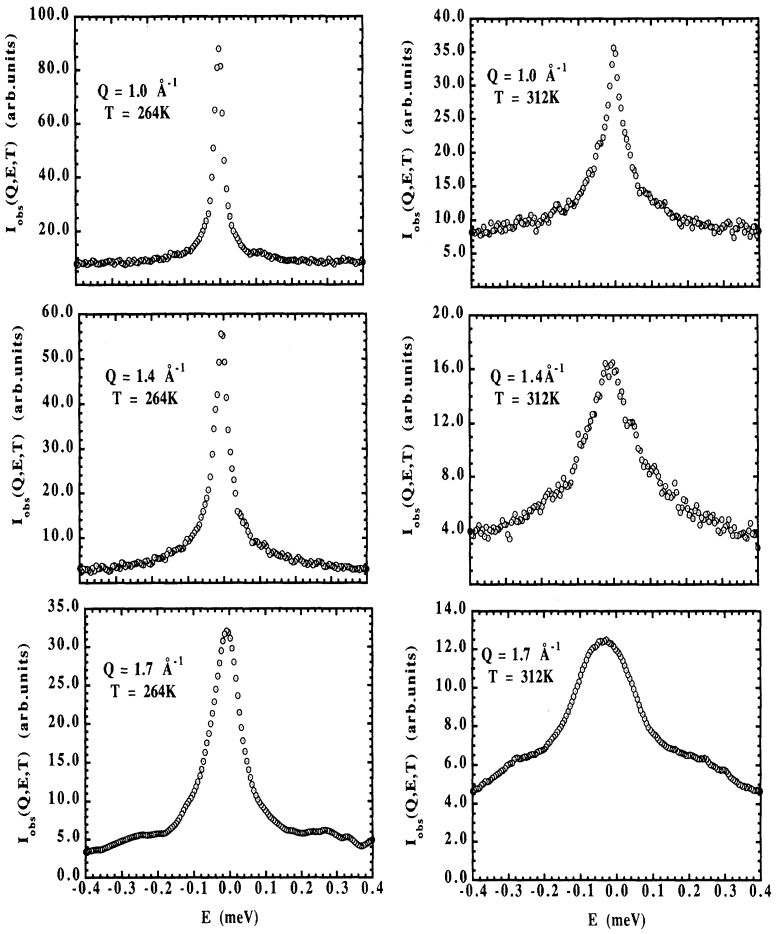

FIG. 1. Corrected quasielastic spectra for two temperatures (264 and 312 K) at both sides of the reported anomaly. Spectra for $Q=1.0$ Å^{-1} correspond to the MI(006) reflection, whereas those for $Q=1.4$ and $Q=1.7$ Å^{-1} are from the PG(002) analyzers, respectively.

vector dependence of $I^{\text{diff}}_{\text{mod}}(Q,E,T)$ is implicit within the molecular form factors, only a global temperature-dependent scaling is needed. On the other hand, due to the lack of any information regarding the inelastic component, both temperature- and wave-vector dependencies are allowed for $a_{\text{inel}}(Q,T)$. The parameters set to be determined from fits to the experimental intensities are thus composed of the $\Gamma_t(Q,T)$ translational linewidth, for which no prespecified assumption is made, the $\Gamma_{\text{inel}}(Q,T)$ inelastic width, and the two above-mentioned scale factors. Such a relatively simple four-parameter model was able to fit satisfactorily all the constant-Q spectra, although small but systematic discrepancies appeared at the largest wave vectors, as will be commented on in Sec. IV.

The temperature dependence of the longitudinal NMR relaxation rates of ^{13}C nuclei given in Table I of Ref. [3] was analyzed in terms of an approach described in detail in Ref [15], where for planar rotators such quantities are expressed in terms of the zeroth-frequency spectral density $J(0)$ as

$$T_1^{-1}(\alpha,T)=BJ(0)=a\cos^2\alpha+b\sin^2\alpha-c\cos^2\alpha\sin^2\alpha\ , \tag{5}$$

where $B=28.5$ ps (relaxation due to dipolar coupling between the carbon nucleus with the directly attached proton) and α stands for an angle between the C—H vector and the principal axis of the rotational diffusion tensor in the molecular plane, which may be substantially displaced from the axis of the free-molecule inertia tensor due to collisional effects. To quantify such an effect, an angle ϕ is defined with respect to some molecule-fixed frame in order to specify the orientation of the principal axes of the rotational diffusion tensor [15] [see Fig. 2(a)]. The equation written above can thus be solved for relaxation data measured for seven different carbon nuclei for each temperature in order to derive values for the angle ϕ and the three a,b,c parameters which are used to calculate the ratios between the elements of the rotational diffusion tensor.

III. RESULTS

A. A reconsideration of already existing data

Before embarking on a detailed analysis of the temperature dependence of the inelastic intensities, we have followed the procedure outlined above to explore if significant changes in the orientational motions occur within the temperature range of interest at time and length scales accessible to NMR spectroscopy.

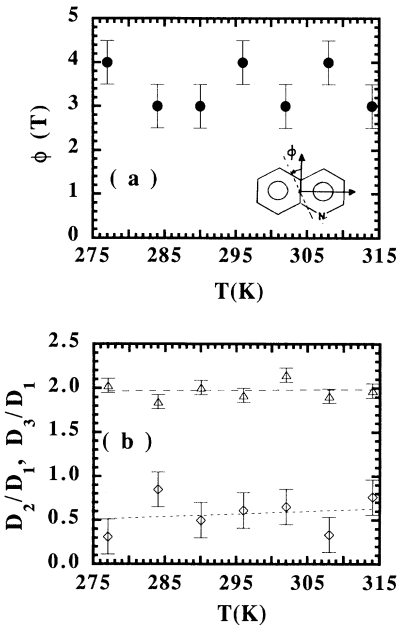

FIG. 2. (a) The temperature dependence of the relative orientation of the angle ϕ as calculated from the least-squares solution of Eq. (6). The inset shows a schematic drawing of the molecular geometry and the orientation of the principal axis. (b) Temperature dependence of the ratios of the rotational diffusion tensor elements D_3/D_1 and D_2/D_1.

As a first result, the relative orientation of the principal axis of the diffusion tensor does not show any significant change within the explored temperature range as can be seen from the derived values of the angle ϕ which are shown in Fig. 2(a). Such a finding indicates that no substantial change has occurred in the geometrical dependence of the reorientational motion within this temperature range, and therefore the changes in relaxation rates should be more sensibly ascribed to changes in the individual values of the rotational diffusion coefficients than to a change in the geometry as a consequence of some geometrical rearrangement. The temperature dependence of the ratios D_3/D_1 and D_2/D_1 are also given in Fig. 2(b) and, as can be seen from the plot, such ratios remain approximately constant within the temperature range of interest. The presence of a weak temperature dependence, as shown by the straight lines in the graphs of Fig. 2(b), cannot be ascertained due to the problem of estimating the ratios from the relaxation rates, which leads to a low statistical accuracy for one of the quantities, as commented on in detail in Ref. [15]. As a matter of fact, only the first of the two ratios can be determined with accuracy from the experimental data, the consequences of which will be commented below. The temperature-dependent quantities

$$D_R(T)=\frac{1}{3}(D_1+D_2+D_3)\ , \tag{6}$$

$$D_s(T)=3(D_1D_2+D_1D_3+D_2D_3) \tag{7}$$

can thus be calculated if an additional independent measurement is available (since only the ratios of the diffusion constants can be derived from the NMR data [15]). For such a purpose, the relaxation time measured by depolarized light scattering $\tau_{LS}=[6D_s-2(9D_s^2-D_R)^{1/2}]^{-1}$ and given in Ref. [4] for the whole temperature range can be used, and the temperature dependence of the three individual constants is shown in Fig. 3(a). From inspection of Fig. 3(a), it can be seen that the values of the rotational constants are close to those found for planar rotators of approximately the same size (see Ref. [15]), being of the order of 10^{10} s.

Once the temperature dependence of D_s and D_R has been established, estimates for an effective correlation time τ_c can be derived, from which the associated rotational diffusion constants $D_r(T)=1/6\tau_c$ entering Eq. (3) are calculated as [16]

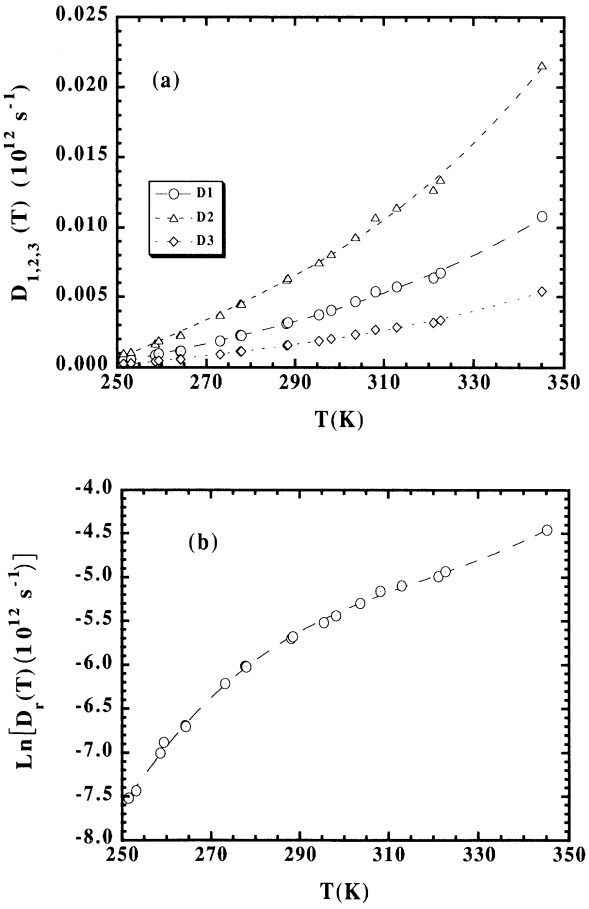

FIG. 3. (a) The temperature dependence of the $D_{1,2,3}$ rotational diffusion constants. (b) A logarithmic plot of the temperature dependence of the effective rotational constant $D_r(T)$. The line joining the experimental points is an interpolating polynomial and is used as a guide to the eye.

$$D_r(T)=\left\{\frac{18}{4D_R}\left[(D_1+D_s)-\left[(D_1-D_2)+\frac{(D_1-D_2)^2}{D_3+D_s}\right]\sin^2\phi+\frac{(D_1-D_2)^2}{D_3+D_s}\sin^4\phi\right]\right\}^{-1}. \quad (8)$$

The values of this reorientational parameter are shown as a semilogarithmic plot in Fig. 3(b), where a noticeable departure from linearity can be seen, evidencing two different motional regimes above and below 285 K, respectively. From data quoted by Chabrat *et al.* [5], derived from independent experimental means for just one value of the temperature, the ratio D_3/D_1 is in agreement with those derived in the present work, whereas somewhat larger values than the average ones found in the present study are quoted for the other ratio (i.e., 0.9 versus 0.65). The relatively large scatter of data points and the absence of any information regarding the temperature dependence of this latter magnitude obviously precludes a more detailed comparison. However, as can be judged from the contribution to the quasielastic linewidths derived from the $D_r(T)$ data shown in Fig. 3(b) [i.e., $\Gamma_r(Q,T)\approx 6$ μeV in the middle of the explored temperature range], such inaccuracies do not constitute a serious obstacle for data analysis purposes following the lines sketched in this work.

Since the details regarding the rotational motion have already been taken care of, the problem thus concerns the analysis of the quasielastic intensities in terms of the translational diffusion and low-energy inelastic components. However, in order to verify if there exists a structural correlate for the observed change in dynamic behavior, a brief examination of the measured x-ray diffraction patterns is indicated.

B. Liquid structure factors

The x-ray patterns for the liquid at temperatures of $T=265$ and 295 K, located on both sides of the reported anomaly, are shown in Fig. 4, where it may be seen that from $Q\approx 1.5$ Å^{-1} onwards the spectra for the two temperatures can be superimposed. The clear double-peak structure is somewhat reminiscent of what has been observed in liquids composed of particles interacting through strong directional forces of electrostatic nature or in those of planar molecules [17]. The characteristic distances associated with the position of the main peak and the subsidiary maximum are 5.7 and 4.2 Å, respectively, which are larger than those corresponding to the longest intramolecular contacts (involving carbon and nitrogen atoms), and therefore can be assigned to distances of preferential orientation of the first neighbors. Such distances are, on the other hand, rather close to those found for the main features exhibited by the carbon-carbon radial distributions in liquid benzene by Claessens, Ferrario, and Ryckaert [17] and are also compatible with estimates of the total pair-correlation function derived from experimental means.

The intensity difference between the two spectra is shown in the inset where it may be seen that a small feature is present at about 1.0 Å^{-1}, which arises from the slightly higher intensity of the spectrum taken at $T=295$ K. Such a temperature dependence could be attributed to a density effect, although the possibility of a small change in the microscopic organization within the liquid cannot be ruled out from the present set of measurements. It should be noticed, however, that the temperature dependence of the structure factor for this liquid seems to evidence a behavior opposite to most molecular (or simple monoatomic) systems where the first diffraction peak loses intensity and broadens as the temperature is raised.

C. Analysis of the quasielastic intensities

The temperature dependence of the integrated quasielastic intensity covering the temperature range of interest is shown in Fig. 5. It seems clear from the graph that two different slopes are apparent for this curve, below and above $T\approx 285$ K, respectively. Since it can be expected that the total integrated intensity of the spec-

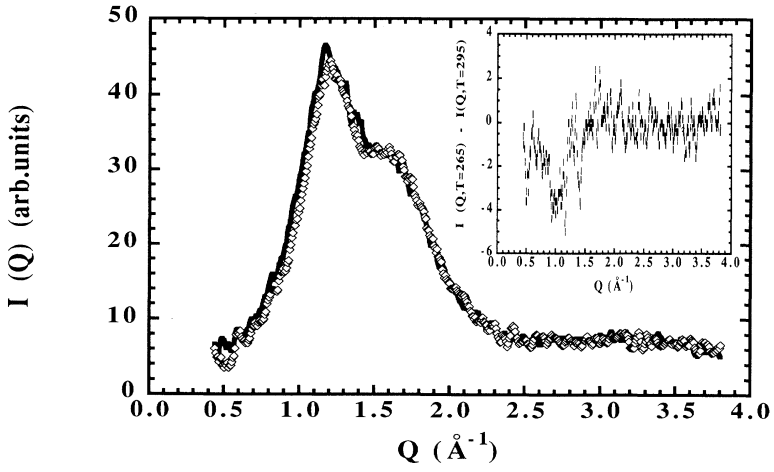

FIG. 4. The x-ray-diffraction patterns for spectra recorded for $T=265$ K (open lozenges) and $T=295$ K (thick solid line). Intensity units are given in counts per second. The inset shows the intensity difference function taken with respect to the spectrum for $T=265$ K.

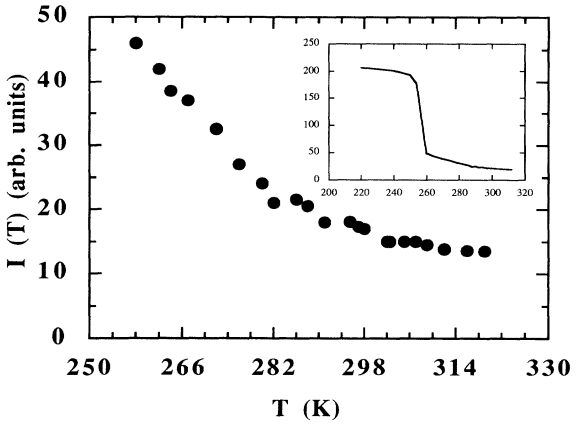

FIG. 5. Temperature dependence of the total (integrated over energy and momentum transfer) quasielastic intensities. The inset shows the variation of this quantity covering the melting transition.

trum (i.e., the zeroth-order moment of the incoherent scattering law evaluated for the whole spectral range) is kept constant with temperature, the most feasible mechanism which can be adduced to explain the observed behavior should concern the transfer of quasielastic intensity to the inelastic wings of the spectrum, which will considerably reduce the integrated intensities for our fixed window of 0.5 meV.

The wave-vector dependence of the $\Gamma_t(Q,T)$ translational linewidths for several temperatures is displayed in Fig. 6. A simple Fickian behavior is followed for momentum transfers below 0.9 Å^{-1}, a significant change in slope occurs for $\sim 1.0 \leq Q \leq \sim 1.4$ Å^{-1}, and a further steep increase in slope then covers the rest of the accessible range of wave vectors.

From the linear (low-Q) part of the curves showing the wave-vector dependence of the translational linewidths, estimates for the $D_T(T)$ self-diffusion coefficient were calculated, and a plot displaying the wave-vector dependence of such quantities is shown in Fig. 7 as a logarithmic representation. No deviations from linearity are observed in all the explored temperature range, and the corresponding values for the Arrhenius parameters are $E_0 = 11.89$ kJ mol^{-1} (≈ 123 meV) for the activation energy and $D_0 = 39.9 \times 10^{-5}$ $\text{cm}^2\,\text{s}^{-1}$ (2.63 meV Å^2) for the frequency factor.

On the other hand, since a smooth behavior in Q is expected, the translational linewidths can be factorized as shown by Eq. (2) and the function $g(Q)$ giving the wave-vector dependence can be parametrized, on empirical grounds, using simple analytical expressions. In the present case, as shown by the lines drawn through the experimental points in Fig. 6(a), a quartic polynomial behavior such as $g(Q) = aQ^2 - bQ^4$ with positive coefficients ($a \gg b$) gives an adequate representation of data for all the explored temperature ranges and momentum transfers up to ≈ 1.3 Å^{-1}.

The $\Gamma_{\text{inel}}(Q,T)$ linewidths characterizing the inelastic response could not be determined accurately at high temperatures since their magnitude becomes comparable with the instrumental energy window [i.e., $\Gamma_{\text{inel}}(Q,T) \approx 0.25$ meV for $Q = 1.4$ Å^{-1} and $T = 312$ K]. For wave vectors above 1 Å^{-1} and for all the explored range of temperatures, $\Gamma_{\text{inel}}(Q,T)$ increases monotonically with momentum transfer, and such inelasticity becomes too weak to be separated from the total spectrum for Q values below 0.9 Å^{-1}. The Q dependence of an estimate of the inelastic intensities, defined as $I_{\text{inel}}(Q,T) = a_{\text{inel}}(Q,T)\Gamma_{\text{inel}}(Q,T)$, is finally shown in Fig. 8(a). The overall shape of the curves is reasonably well accounted for in terms of a simple model for the inelastic

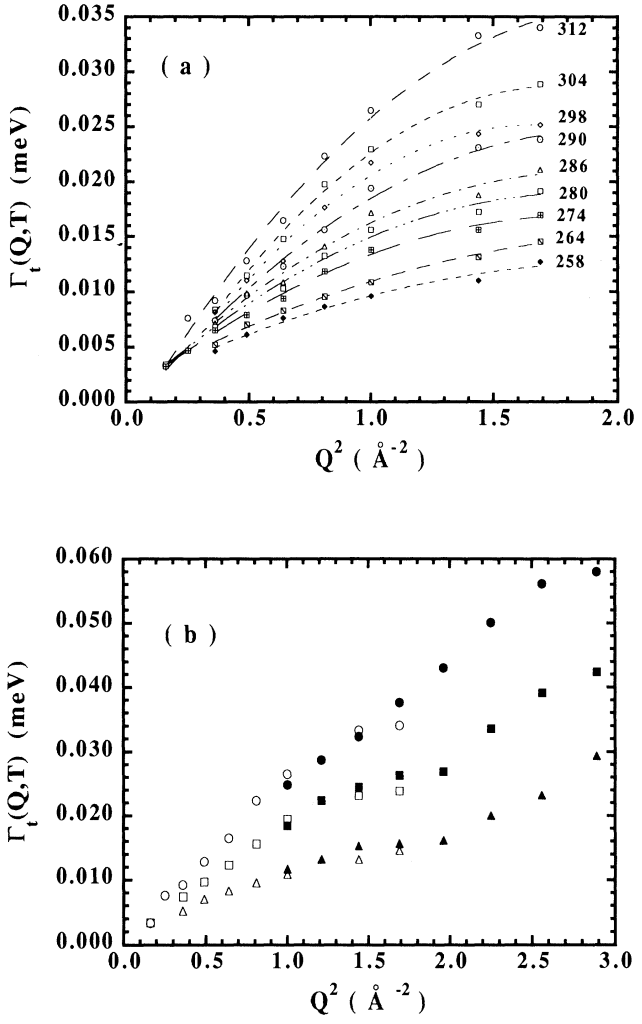

FIG. 6. (a) Temperature and wave-vector dependence of the translational linewidths $\Gamma_t(Q,T)$ as estimated from spectra measured using the MI006 reflection. The figures at the upper right ends of the curves label the temperature for each data set. The lines joining the experimental points correspond to values of the $g(Q)$ functions (see text). (b) A comparison of the translational linewidths as measured using the MI006 (open symbols) and PG002 (filled symbols) analyzer reflections. Temperatures correspond to 312 K (circles), 290 K (squares), and 264 K (triangles).

intensities, defined as $I_{\text{inel}}(Q,T)=a_{\text{inel}}(Q,T)\Gamma_{\text{inel}}(Q,T)$, is finally shown in Fig. 8(a). The overall shape of the curves is reasonably well accounted for in terms of a simple model for the inelastic intensity of a particle harmonically bound to a body freely diffusing in the fluid. In such a case, the integrated intensity of the quasielastic spectrum can be written as [18]

$$I_{\text{inel}}(Q,T)\propto \exp[-2W(Q)]I_0(\hbar Q^2/[2M_{\text{eff}}\omega_0\sinh(\hbar\omega_0/2k_BT)]) ,$$
$$2W(Q)=(\hbar Q^2/2M_{\text{eff}}\omega_0)\coth(\hbar\omega_0/2k_BT) , \tag{9}$$

where the exponential is a Debye-Waller term, $I_0(\ )$ stands for a modified Bessel function, M_{eff} stands for the effective mass of the particle executing the harmonic motion, ω_0 its characteristic frequency, and the rest of the symbols retain their usual meaning. It should be noticed that the curvature of the plots is governed by the effective mass, the oscillation frequency, and temperature only, and therefore the comparison between experimental and calculated quantities is meaningful even if the former are expressed in a relative scale. Some multiexcitation contributions could also be present in the inelastic background, and their relative importance can be estimated from the expected Q^4 dependence of their intensity. Although an accurate separation of such contributions from the inelastic single-excitation intensity cannot be sensibly attempted with the present data, a semiquantitative estimation can be accomplished supplementing the equation given above with a term $a_{\text{mult}}(T)Q^4$. Estimates of such multiexcitation contributions performed in such a way range from 5.2% of the total inelastic intensity at $T=270$ K up to $\sim 7\%$ for $T=304$ K, as shown in the inset of Fig. 8(a). The nonmonotonic shape of the curve showing the multiexcitation intensity versus temperature was somewhat unexpected and may indicate some coupling with the other three adjustable parameters.

The values for the effective masses for the whole range of temperatures, as calculated from fits to the formula written above, are shown in Fig. 8(b) in terms of the molecular mass (1 Mmol $\approx$129 amu). A clear break in the behavior of the temperature dependence of this magnitude is clearly seen to occur at about 290 K, and at high enough temperatures it seems to approach the single-molecule value. On the other hand, the oscillation frequency only shows a weak linear dependence with temperature and its values are bounded within the interval 0.11 meV (270 K) $\leq\omega_0\leq$ 0.12 meV (312 K).

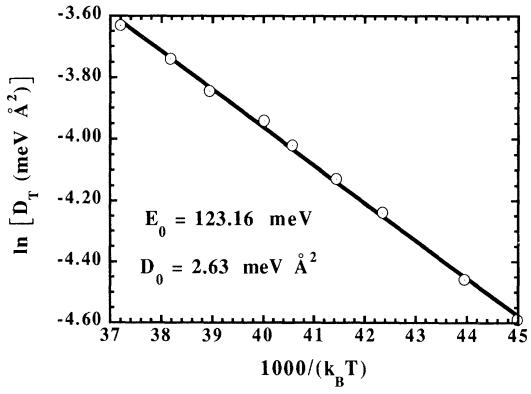

FIG. 7. Temperature dependence of the logarithm of the translational diffusion coefficient as estimated from the low-Q part of the $\Gamma_t(Q,T)$ curves. The experimental data are represented by the open circles and the thick solid line gives the best approximation to an Arrhenius law with parameters values given in the figure (see text).

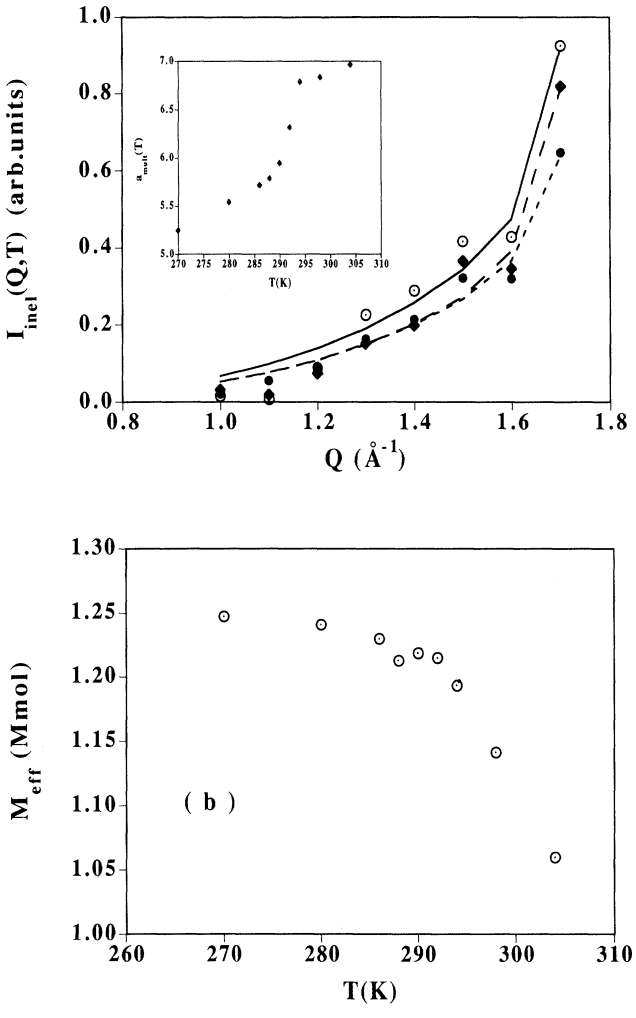

FIG. 8. (a) Wave-vector dependence of the $I_{\text{inel}}(Q,T)$ inelastic intensities for several temperatures. Open circles and the solid line represent experimental data for $T=304$ K as well as the approximation given by Eq. (9), filled lozenges and the long-dashed line correspond to $T=280$ K, and filled circles with the dashed line to $T=264$ K. The inset shows the temperature dependence of $a_{\text{mult}}(T)$ given in percentage units of the total intensity. (b) The temperature variation of the effective masses given in terms of the free molecule mass Mmol.

IV. DISCUSSION

Before starting to discuss the results described in the preceding section let us briefly enumerate the main findings of the present work.

(i) No significantly large change in the liquid structure occurs within the explored temperature range. The observed intensity difference between the two extreme temperatures shown in Fig. 4 could perhaps be explained as a density effect (i.e., the looser packing of the liquid shifts the first peak towards smaller wave vectors), although a definite explanation would require data of far higher accuracy.

(ii) The rotational motion shows within this range of temperatures a clear nonlinear behavior, something which apart from the recent NMR evidence [3] is also substantiated by the depolarized light scattering data of Ref. [4].

(iii) In contrast, the experimental estimates of the $D_t(T)$ translational diffusion coefficient show a clear Arrhenius behavior, and both the individual values of the coefficients as well as their activation parameters are in agreement with estimates for other systems composed of planar molecules [19].

(iv) A clear inelastic background is apparent at all the explored temperatures within the liquid range but disappears on freezing. The strong wave-vector dependence suggests the presence of a harmonic, albeit strongly damped (or overdamped) component.

From the fitted $I_{\rm mod}(Q,E,T)$ functions, estimates of the low-frequency part of the $Z(E)$ generalized frequency distributions (i.e., for excitations below a cutoff energy E_c dictated by kinematical restrictions) were obtained following standard procedures [20]. Once such quantities were evaluated, an estimate of their contribution to the total specific heat was calculated as

$$\Delta C(E_c,T)\approx\int_0^{E_c}dx\,x^2\frac{\exp(x)}{[\exp(x)-1]^2}Z(E)\ , \qquad (10)$$

with $x=\hbar\omega/k_BT$, where the upper limit of the integral was first taken to be 0.5 meV, corresponding to the allowable experimental range of energy transfers. A plot of the temperature dependence of $\Delta C(E_c,T)$ is shown in Fig. 9. Because of the very limited range of energy transfers, normalization of this quantity to an absolute scale [i.e., after normalization to unity of the total $Z(E)$], obviously becomes impracticable. However, our interest here is focused on the temperature dependence and therefore the comparison may be carried out on a relative scale. The most relevant feature arising from such an exercise regards the strong temperature dependence of $\Delta C(E_c,T)$, since $E_c=0.5$ meV ≈ 5.8 K relative to the temperature range of interest of 260–312 K. The shape of such a curve can be understood on the basis of a significant transfer of intensity towards higher frequencies as the temperature is raised, which leads to an increase in specific heat since the very low frequencies do not contribute significantly to $\Delta C(E_c,T)$ [i.e., $Z(E)\approx E^2 I_{\rm mod}(Q,E,T)$ and therefore their weight to the integral written above is rather small]. At temperatures around 300 K and above the transfer of intensity to the inelastic wings is responsible for the plateaulike shape of the curve, a feature which is clearly related to the finite energy window of the experiment. In addition, and to explore the dependence of such curve with the value of the E_c energy cutoff, the inset in Fig. 9 represents the same quantity evaluated using $E_c=1$ meV (i.e., extrapolating the model fits up to that value of the energy transfer). As can be seen from the inset, the strong dependence with temperature is maintained and some hints of a change in slope about 280 K, reminiscent of those found in Ref. [3], are apparent as shown by the two straight lines. However, additional experimental data covering a larger energy-transfer range are needed to assess the validity of such extrapolation.

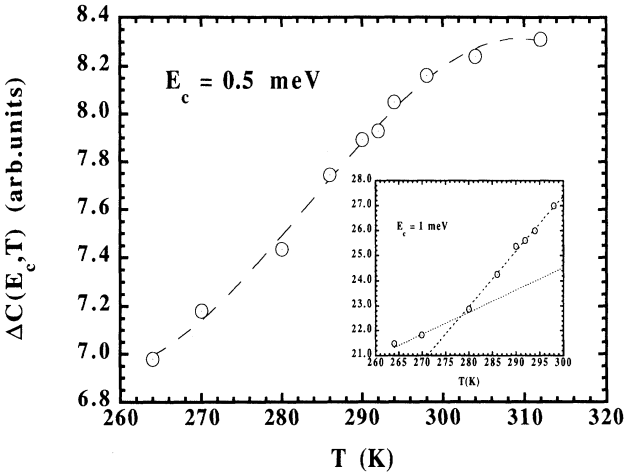

FIG. 9. Temperature dependence of the $\Delta_c(E_c,T)$ contribution to the harmonic constant volume specific heat arising from excitations with frequencies below E_c. The inset shows the result of extrapolating the data up to 1 meV (see text).

In order to shed some light on the origin of the inelastic background, consideration was made of the results derived by Wang [7] from a calculation carried out in terms of the generalized Langevin equation approach for a dynamical variable formed by components of the translational momentum density and their complex conjugates, and those of Quentrec [1] where use is made of some microscopic information regarding the center of mass and orientational order within the fluid.

Although the results were only developed to work within the hydrodynamic region, their implications for larger Q values can be justified in the same way as employed in calculations of this kind for other dynamical variables (i.e., making explicit the wave-vector and frequency dependence of the relevant transport coefficients). Once this proviso is made we shall note that in both calculations the quantity giving the damping constant of the shear wave $\eta=Q^2\eta_s/2\pi\rho$, where η_s stands for the static value of the shear viscosity and ρ is the mass density, governs the passage from the propagative to diffusive regimes. In particular, a useful criterion for delimiting both regimes is given in terms of a parameter R, which is normalized to unity and gives the strength of the coupling between shear and rotational excitations (i.e., $R=0$

implies that the fluid behave as a Newtonian body whereas $R=1$ indicates a Maxwellian behavior characterized by a single relaxation time τ_M) as [1]

$$B_1<\eta\tau_{\mathrm{LS}}<B_2\ ,$$
$$B_1=\frac{(1-R^{1/2})^2}{(1-R)^2}\ , \tag{11}$$
$$B_2=\frac{(1+R^{1/2})^2}{(1+R)^2}\ ,$$

where the propagative behavior implies that the product $\eta\tau_{\mathrm{LS}}$ is within bounds B_1 and B_2 and overdamped behavior otherwise. From values of the shear viscosity and density taken from [4] at $T=293$ K and estimates of $R\approx 0.6$ given by Frölich and Posch [21], it becomes clear that even in the limit of long wavelengths at temperatures well above melting the transverse modes are heavily damped ($B_1=0.3, \eta\tau_{\mathrm{LS}}=0.1$), and therefore no clear finite-frequency features are observable in the spectrum of scattered light. The important point to note is the fact that the relatively large value of R (≈ 0.6 at temperatures about $T=290$ K decreasing when the temperature is raised to ~ 0.53 at $T=308$ K [5,21]) implies that the coupling of the thermal shear to reorientational motions does constitute an efficient mechanism to relieve microscopic stresses by means of fast reorientational fluctuations.

Although it is not expected to observe the spectrum of shear excitations in the kinematic range accessible to neutron scattering from a mostly incoherent sample, its effect on the reorientational motions may explain the origin of the strong inelastic background measured in the present set of experiments. What is somewhat remarkable is the fact that the widths of the inelastic component (of the order of 0.1–0.3 meV) can be compared with the values of the correlation times for vibrational dephasing, $\tau_c=0.3$ ps≈ 0.2 meV derived from the analysis of infrared and Raman band contours of the same material [22], evidencing characteristic times far shorter than those involved in molecular reorientations or long-range translational diffusion. Furthermore, the fact that the collision rate derived from such correlation times increases by a factor of 3–4 after crystallization [22] suggests that the origin of such a feature is related to some mechanism where the acoustic phonons are coupled to localized librations.

From consideration of the ω_0 frequencies derived from the analysis of the inelastic intensities, and extrapolating the shear wave frequency from data given in Ref. [4] for $T=295$ K to the value of the momentum transfer where it is expected to show its maximum value which corresponds to a wave number of $Q_p/2=0.5$ Å^{-1} [23] [halfway to the Q value corresponding to the maximum of the first peak of $S(Q)Q_p$ [24]] an upper bound of 0.8 meV is found. For larger values of the momentum transfer such a frequency should exhibit some oscillations with a minimum located about Q_p. Therefore it may be expected that the shear wave frequencies become close to the ω_0 estimated from the analysis of the inelastic intensities which are of ~ 0.1 meV, something which would enable an efficient resonance coupling between shear and fast reorientational motions.

An additional indication of the coupling referred to above is constituted by the fact that a linear fit of the shear frequency versus temperature from data reported by Rouch *et al.* [5] indicates that the crossover from propagating to diffusive regimes occur about $T=285$ K, which basically coincides with the temperature where the change in slope of several dynamical quantities is manifested [3].

In the absence of any other feasible mechanism able to originate such inelastic feature [24,25], and also based upon the facts that all other transport properties such as the mass diffusion coefficient and the sound velocity [4] behave linearly as characteristic of most (simple) liquids, it seems clear that the observed feature should be attributed to fast reorientational librations which are excited by the coupling of the orientational degrees of freedom to thermally excited shear waves. The fact that such an effect remains visible well within the kinematical range accessible to cold neutron spectroscopy once more evidences the microscopic origin of such phenomena, and therefore, further inelastic neutron-scattering experiments covering a larger range of energy transfers as well as computer molecular-dynamics simulations are called for in order to unravel the fine details regarding the microscopic dynamics of this interesting liquid.

V. CONCLUSIONS

The intricate dynamical effects studied for about two decades within the hydrodynamic limit by means of depolarized Rayleigh scattering are found to have a clear correlate at microscopic scales as it is evidenced by the incoherent high-energy resolution inelastic neutron spectra. To the authors knowledge, no other molecular liquid has been shown to exhibit, at these length and time scales, a similar phenomenology.

Several quantities derived from the spectra seem to reproduce a change in dynamical behavior about $T=290$ K, something which may constitute a microscopic correlate of those phenomena observed at macroscopic scales such as the change in slope of the reorientational correlation time as measured by light scattering, NMR relaxation, or even the specific heat.

Further work employing structural analogs (i.e., isoquinoline) and molecular-dynamics simulations using highly refined interparticle potentials are deemed necessary in order to delve into a truly microscopic understanding of the origin of the thermal anomalies studied in this work.

ACKNOWLEDGMENT

This work has been supported in part by DGICYT Grant No. PB89-0037-C03.

[1] B. Quentrec, J. Phys. (Paris) **9**, 1 (1984).

[2] E. W. Fischer, Proceedings of the Workshop on Dynamics of Disordered Materials II [Physica A (to be published)].

[3] D. Jalabert, J. B. Robert, H. Roux-Buisson, J. P. Kintzinger, J. M. Lehn, R. Zinzius, D. Canet, and P. Tekely, Europhys. Lett. **15**, 435 (1991). Additional calorimetric measurements can be found in W. V. Steele, D. G. Archer, R. D. Chirico, W. B. Collier, I. A. Hosenlopp, A. Nguyen, N. K. Smith, and B. E. Gammon, J. Chem. Thermodyn. **20**, 1233 (1988).

[4] G. I. A. Stegeman and B. P. Stoicheff, Phys. Rev. A **7**, 1160 (1973).

[5] The data regarding the temperature dependence of the shear frequencies were taken from Table II of J. Rouch, J. P. Chabrat, L. Letamendia, C. Vaucamps, and N. D. Gershon, J. Chem. Phys. **63**, 1383 (1975); see also Mol. Phys. **30**, 963 (1995); J. P. Chabrat, L. Letamendia, J. Rouch, and C. Vaucamps, *ibid.* **28**, 81 (1994). A study of the pressure dependence of the spectrum of depolarized scattered light is given in P. Frölich and H. A. Posch, *ibid.* **36**, 1421 (1978).

[6] G. D. Enright and B. P. Stoicheff, J. Chem. Phys. **64**, 3658 (1976).

[7] C. H. Wang, Mol. Phys. **41**, 541 (1980), gives an account of the application of the Mori-Zwanzig technique to liquid salol.

[8] S. M. Rytov, Zh. Eksp. Teor. Fiz. **33**, 514 (1958) [Sov. Phys.—JETP **6**, 401 (1958)]. For more recent developments cast in terms of linear irreversible thermodynamics see, for instance, R. F. Rodriguez, O. Manero, and M. Aguado, Phys. Rev. B **38**, 4827 (1988). See references in this latter paper for a general update.

[9] Rutherford Appleton Laboratory computer software package.

[10] J. Alonso, M. García-Hernandez, F. J. Bermejo, and J. L. Martinez, Institut Laue Langevin Technical Report No. 91AL01T, 1991 (unpublished).

[11] M. W. Johnson, AERE Report No. 5697, 1974 (unpublished).

[12] An adaptation of the code developed by F. Rieutord (Institut Laue Langevin) for dealing with inverted geometry spectrometers was carried out.

[13] V. F. Sears, Can. J. Phys. **45**, 237 (1966).

[14] The relevant parameters needed for the calculation of the molecular form factors were computed from molecular structures optimized using standard theoretical chemistry tools. The functions needed to specify the model are then $f^2_{\text{incoh}}=\sum_{i=1}^{17}(b^i_{\text{incoh}})^2 j_0^2(Qr_i)$ and $\chi_l(Q)=\sum_{i=1}^{17}(b^i_{\text{incoh}})^2 j_l^2(Qr_i)$, where the b^i's are scattering lengths and $J_l(Qr_i)$ are spherical Bessel functions given in terms of arguments containing the r_i distances to the molecular center of mass.

[15] E. Diez, F. J. Bermejo, and J. Guilleme, J. Chem. Phys. **83**, 58 (1985).

[16] J. McConnell, *The Theory of Nuclear Magnetic Relaxation in Liquids* (Cambridge University Press, Cambridge, 1987), p. 85.

[17] The structure factor of a dense dipolar liquid is described by M. Alvarez, F. J. Bermejo, P. Chieux, E. Enciso, M. García-Hernandez, and N. Garcia, Mol. Phys. **66**, 397 (1989). A characteristic double peak in the first diffraction maximum is also shown in liquids composed by planar molecules such as tetrachloroethylene: M. Alvarez, F. J. Bermejo, P. Chieux, E. Enciso, J. Alonso, and N. Garcia, J. Phys. Condens. Matter **1**, 8595 (1989); or benzene: E. Bartsch, H. Bertagnolli, G. Schulz, and P. Chieux, Ber. Bunsenges. Phys. Chem. **89**, 147 (1985). Results from a molecular-dynamics simulation of liquid benezene are given by M. Claessens, M. Ferrario, and J. P. Ryckaert, Mol. Phys. **50**, 217 (1983).

[18] S. W. Lovesey, *Theory of Neutron Scattering from Condensed Matter* (Oxford Science Publications, Oxford, 1986), p. 244.

[19] See, for instance, F. P. Ricci, in *Molecular Liquids: Dynamics and Interactions,* Vol. 135 of *NATO Advanced Study Institute, Series B: Physics,* edited by A. J. Barnes *et al.* (Reidel, Dordrecht, 1984), p. 35.

[20] See, for instance, A. Chahid, M. García-Hernandez, C. Prieto, F. J. Bermejo, E. Enciso, and J. L. Martinez, Mol. Phys. **78**, 821 (1993).

[21] From data compiled by Frölich and Posch [5]. The estimated values for this quantity vary from $R=0.66$ at $T=285$ K to $R=0.53$ at $T=305$ K.

[22] W. G. Rothschild, J. Chem. Phys. **65**, 455 (1976).

[23] Although the spectrum of transverse current fluctuations cannot be easily measured for a liquid, estimates of the frequency dispersion can be obtained by simulational means. As an example, the wave-vector dependence for the shear frequency in a complex liquid is given by J. Alonso, F. J. Bermejo, M. García-Hernandez, J. L. Martinez, W. S. Howells, and A. Criado, J. Chem. Phys. **96**, 7696 (1992), and a comparison with polycrystal data in Phys. Lett. A **172**, 177 (1992).

[24] The macroscopic shear viscosity and the density decrease with temperature in a quasilinear fashion within the temperature range we are interested in. Taken from Rouch *et al.* and Frölich and Posch [5].

[25] Other plausible mechanisms such as collective reorientational motions are ruled out since from simple mass arguments they should occur at lower frequencies (i.e., below that characteristic of single-molecule rotations), and therefore can only contribute to the low-energy quasielastic region of the spectrum.